

# Full-degrees-of-freedom frequency based substructuring

Armin Drozg<sup>a</sup>, Gregor Čepon<sup>a,\*</sup>, Miha Boltežar<sup>a</sup>

<sup>a</sup>*Faculty of mechanical engineering, University of Ljubljana*

---

## Abstract

Dividing the whole system into multiple subsystems and a separate dynamic analysis is common practice in the field of structural dynamics. The substructuring process improves the computational efficiency and enables an effective realization of the local optimization, modal updating and sensitivity analyses. This paper focuses on frequency-based substructuring methods using experimentally obtained data. An efficient substructuring process has already been demonstrated using numerically obtained frequency-response functions (FRFs). However, the experimental process suffers from several difficulties, among which, many of them are related to the rotational degrees of freedom. Thus, several attempts have been made to measure, expand or combine numerical correction methods in order to obtain a complete response model. The proposed methods have numerous limitations and are not yet generally applicable. Therefore, in this paper an alternative approach based on experimentally obtained data only, is proposed. The force-excited part of the FRF matrix is measured with piezoelectric translational and rotational direct accelerometers. The incomplete moment-excited part of the FRF matrix is expanded, based on the modal model. The proposed procedure is integrated in a Lagrange Multiplier Frequency Based Substructuring method and demonstrated on a simple beam structure, where the connection coordinates are mainly associated with the rotational degrees of freedom.

*Keywords:* Piezoelectric rotational accelerometer, rotational degrees of freedom, experimental modal analysis, modal shape slopes, FRF synthesis, experimental frequency based substructuring

---

\*Corresponding author

*Email address:* `gregor.cepon@fs.uni-lj.si` (Gregor Čepon)

## 1. Introduction

The methodology to divide large and complex systems into smaller subsystems is common practice in the field of structural dynamics. Analyzing a subsystem's dynamics separately, results in less complexity and a higher computational efficiency. The dynamic properties can be obtained experimentally or numerically. Whenever the system is modified, the dynamic analysis is reduced only to the given subsystem, which is then merged with the rest of the structure using a dynamic substructuring (DS) process. By using DS methods it is possible to effectively perform a local optimization, modal updating and sensitivity analyses.

Classically, the DS methods can be divided into three subclasses. The first, so-called Component Mode Synthesis (CMS), is based on the modal parameters. The second one, Impulse Based Substructuring (IBS), is the youngest in the family of substructuring methods and is based on the Impulse-Response Functions (IRFs). The last one, Frequency Based Substructuring (FBS), uses the response model within a coupling process. The FBS is normally based on experimental data as there is a possibility to directly measure the Frequency Response Functions (FRFs). Within FBS several methods have been developed; however, until recently, they have not gained much popularity. In 2006, the Lagrange Multiplier Frequency Based Substructuring (LM FBS) method was introduced by de Klerk et al. [1]. It represents a reformulated version of the admittance FBS method proposed by Jetmundsen et al. [2]. In order to obtain a full-degrees-of-freedom (DOF) FRF matrix, the measurement of translational as well as rotational responses must be performed. This can be done effectively if the FRFs are obtained from a numerical model; however, it still represents a problem whenever the FRFs are obtained solely by experiment. One of the main difficulties is to measure the rotational DOF; thus, it is not possible to obtain the full FRF matrix, which may lead to erroneous results during the substructuring process.

There have been various attempts to excite structures with a pure moment and observe the rotational responses. Some researchers proposed the finite-differences theory, together with precisely positioned translational accelerometers [3, 4] to measure the rotational DOFs. Several attempts were made to excite the structure indirectly with the moment by using T-blocks, the finite-differences method or two synchronous impact hammers [5–7]. The development of a rotational sensor based on bimorph materials is presented

in [8]. A method to deduce the rotational modal shapes by measuring the strains is shown in [9]. Despite extensive research in this field, the presented methods have limitations and are not yet generally applicable. Thus, some researchers try to combine experimental and numerical approaches [10, 11] in order to improve/update the measurements. In some cases the rotations are not even considered in the coupling process [11, 12] and only the translational DOFs are used.

The objective of this paper is to present the substructuring process based on an experimentally obtained, full-DOF response model together with the LM FBS method. The rotations are measured using a quartz-based piezoelectric rotational accelerometer that is well established in the car-safety testing industry [13], although it has not yet gained much popularity in the field of experimental modal analysis (EMA). In order to obtain the full-FRF matrix during the substructuring process it is necessary to measure the excitation force as well as the excitation moment. In this paper an alternative approach is proposed where the moment-excited part of the FRF matrix is deduced based on the introduction of the modal model. To generate a complete response model, modal shapes and not generally considered modal-shape slopes will be included in the FRF synthesis algorithm. Moreover, with the curve-fitting process, the procedure makes it possible to smooth the response functions, which additionally improves the quality of the substructuring process.

The following section briefly summarizes the LM FBS method. In Section 3, the inclusion of the rotational degrees of freedom into the response and modal model will be presented. The fourth section presents the characteristics of a piezoelectric rotational accelerometer and, finally, the applicability of the developed method is demonstrated on a simple beam structure.

## 2. LM FBS method

The LM FBS method requires the full-DOF FRF matrix and the evaluation of the compatibility conditions. The FRFs represent the dynamic stiffnesses between an arbitrary combination of the DOF on the subsystems. With compatibility conditions, one uniquely defines the mutual connections between the subsystems. The theory in this section summarizes the work of de Klerk et al. [1].

The dynamics of an arbitrary subsystem  $s$  can be theoretically determined by the equation of motion in the time domain as:

$$\mathbf{M}^{(s)} \ddot{\mathbf{u}}(t)^{(s)} + \mathbf{C}^{(s)} \dot{\mathbf{u}}(t)^{(s)} + \mathbf{K}^{(s)} \mathbf{u}(t)^{(s)} = \mathbf{f}(t)^{(s)}, \quad (1)$$

where  $\mathbf{M}^{(s)}$ ,  $\mathbf{C}^{(s)}$  and  $\mathbf{K}^{(s)}$  represent the mass, damping and stiffness matrices of subsystem  $s$ , respectively. The variable  $\mathbf{f}^{(s)}$  stands for the force excitation vector of the subsystem. Using a Fourier transformation, Eq. (1) can be transformed into the frequency domain as:

$$[-\omega^2 \mathbf{M}^{(s)} + j\omega \mathbf{C}^{(s)} + \mathbf{K}^{(s)}] \mathbf{U}(\omega)^{(s)} = \mathbf{F}(\omega)^{(s)}, \quad (2)$$

where  $\mathbf{U}^{(s)}$  generally stands for the displacement, velocity or acceleration vector. Eq. (2) can be further rewritten as:

$$\mathbf{Z}(\omega)^{(s)} \mathbf{U}(\omega)^{(s)} = \mathbf{F}(\omega)^{(s)}, \quad (3)$$

where

$$\mathbf{Z}(\omega)^{(s)} = [-\omega^2 \mathbf{M}^{(s)} + j\omega \mathbf{C}^{(s)} + \mathbf{K}^{(s)}], \quad (4)$$

stands for the dynamic stiffness matrix. The mass, damping and stiffness matrices are not separately available when dealing with experimentally obtained data. Thus, Eq. (3) needs to be reformulated in the form:

$$\mathbf{Y}(\omega)^{(s)} \mathbf{F}(\omega)^{(s)} = \mathbf{U}(\omega)^{(s)}, \quad (5)$$

where  $\mathbf{Y}(\omega)^{(s)}$  is the subsystem's response matrix ( $\mathbf{Y} = \mathbf{Z}^{-1}$ ). The response matrix contains all the combinations of FRFs between the input excitation and the output response points. These are used in a dual manner formulated LM FBS method.

The coupling process based on the FRF matrix also requires compatibility conditions. The Boolean mapping matrix  $\mathbf{B}$  defines the subsystems mutual relationship at the connection points. For rigid joint connections, the compatibility matrix is defined as:

$$\mathbf{B}\mathbf{U} = \mathbf{0}. \quad (6)$$

Implementing the compatibility condition in Eq. (3) results in:

$$\mathbf{Z}\mathbf{U} + \mathbf{B}^T \boldsymbol{\lambda} = \mathbf{F}, \quad (7)$$

where  $\boldsymbol{\lambda}$  are Lagrange multipliers representing the connection joints forces. the final matrix notation of the dual assembled system is a combination of Eqs. (6) and (7):

$$\begin{bmatrix} \mathbf{Z} & \mathbf{B}^T \\ \mathbf{B} & \mathbf{0} \end{bmatrix} \begin{pmatrix} \mathbf{U} \\ \boldsymbol{\lambda} \end{pmatrix} = \begin{pmatrix} \mathbf{F} \\ \mathbf{0} \end{pmatrix}. \quad (8)$$

Eliminating  $\boldsymbol{\lambda}$  from Eq. (8) returns the final response matrix of the coupled subsystems:

$$\mathbf{Y}^{(tot)} = \mathbf{Y} - \mathbf{Y}\mathbf{B}^T(\mathbf{B}\mathbf{Y}\mathbf{B}^T)^{-1}\mathbf{B}\mathbf{Y}. \quad (9)$$

### 3. Combination of the response and modal model

The LM FBS method is based on a full-DOF response model. The subsystem's dynamics can be obtained numerically or experimentally. It is also possible to update the numerical model with measurements, or vice versa. The purpose of this paper is to perform a substructuring process based on experimentally obtained data. A complete response model requires measurements of the translations and rotations, as well as the force and moment excitations. The measurement of the translational response is already well established in the field of EMA; however, here we have additionally performed measurements of the rotations using a quartz-based, piezoelectric, rotational accelerometer. As force-excited structural responses represent only the left-hand part of the FRF matrix it is necessary to also obtain the right-hand moment-excited part of the FRF matrix. Because it is difficult to apply a pure moment excitation, here an alternative approach is proposed, where the moment-excited part in the FRF matrix is deduced based on the introduction of the modal model. If it is possible to measure at least one full column in the FRF matrix, the modal parameters can be obtained using well-established modal parameter estimation (MPE) methods. Thus, the required full-DOF FRF matrix can be finally obtained, based on estimated modal parameters. The proposed procedure, which is schematically presented in Fig. 1, enables the reconstruction of unmeasured data and additionally the smoothing of the response functions.

As the inclusion of rotations expands the response and modal domain formulations, a brief explanation of both will be presented [14, 15]. The response model introduces the FRFs that represent the relationship between the excitation and the response point as:

$$\mathbf{X}(\omega) = \mathbf{H}(\omega) \mathbf{F}(\omega), \quad (10)$$

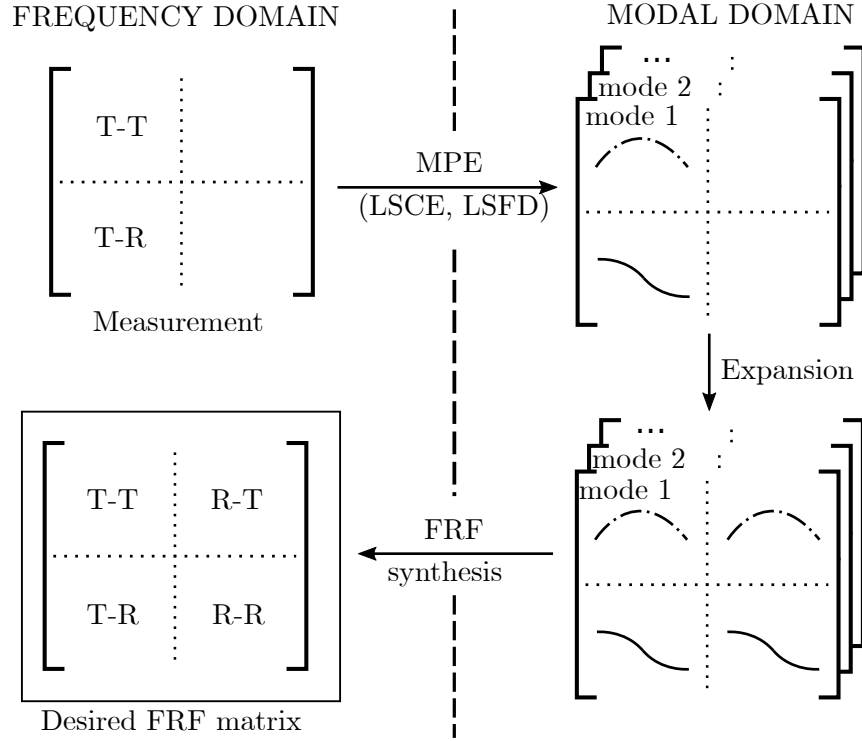


Figure 1: Process of obtaining full degrees of freedom FRF matrix.

where  $\mathbf{X}(\omega)$  represents the response vector,  $\mathbf{H}(\omega)$  is the FRF matrix and  $\mathbf{F}(\omega)$  is the excitation vector in the frequency domain. Whenever the excitation and the response are at the same point on the structure, the FRF represents the driving point response function and the transfer response function when they differ. The matrix  $\mathbf{H}(\omega)$  in Eq. (10) can be divided into three parts: lower residuals (LR), flexible modes (FM) and upper residuals (UR). Because each mode contributes a portion to the final response function, none of them should be omitted. The expanded formulation of the system response function including all the translational and the rotational degrees of freedom can be written as:

$$\begin{aligned} \mathbf{H}(\omega) &= \begin{Bmatrix} \mathbf{H}(\omega)_{T_{dof}} \\ \mathbf{H}(\omega)_{R_{dof}} \end{Bmatrix} = \\ &= \begin{Bmatrix} \{\text{LR}\}_{T_{dof}} \\ \{\text{LR}\}_{R_{dof}} \end{Bmatrix} + \begin{Bmatrix} \{\text{FM}\}_{T_{dof}} \\ \{\text{FM}\}_{R_{dof}} \end{Bmatrix} + \begin{Bmatrix} \{\text{UR}\}_{T_{dof}} \\ \{\text{UR}\}_{R_{dof}} \end{Bmatrix}. \end{aligned} \quad (11)$$

In general, each node on the continuous system consists of six DOFs or at least one translation and an associated rotation for simplified one-dimensional systems. Combinations between the translational and rotational DOFs can be presented by defining four parts in the FRF matrix:

$$\mathbf{H}(\omega) = \begin{bmatrix} \text{T-T} & \text{R-T} \\ \text{T-R} & \text{R-R} \end{bmatrix}. \quad (12)$$

The left-hand part of the FRF matrix represents the force-excited and the right-hand part, the moment-excited FRFs. Translational responses are located on the upper part and rotations on the lower part of the FRF matrix. The full DOF FRF matrix, where all the experimental points on the structure are defined by six DOFs, is rarely used in the field of experimental dynamics. Usually, only the upper left-hand quarter is used as it is difficult to obtain reliable measurements of the FRF associated with rotations.

In this paper the complete left-hand part of the  $\mathbf{H}(\omega)$  matrix is obtained from the measurements (see Fig. 1 (Stage 1)). As it is also necessary to obtain the right-hand part, the modal model is additionally introduced into the analysis. With advanced poly-reference MPE methods, such as the least-square complex exponential (LSCE) or the least-square frequency domain (LSFD), we can accurately estimate the modal parameters. The LSFD method is also capable of estimating the lower and upper residuals.

The system's dynamic properties in the modal domain are defined by the modal parameters. Modal shapes are well established; however, the modal-shape slopes are not frequently used within EMA. They represent a slope or first derivatives of classical modal shapes. There are some methods to obtain modal-shape slopes by a derivation of the modal shapes [16, 17], nevertheless this procedure is very sensitive to small errors and noise in the modal shapes and can lead to a meaningless result after the derivation. Thus, it is essential to directly measure the rotational DOFs on the structure itself. Fig. 1 (Stage 2) shows typical mode-shape vectors for a simple beam structure that can be extracted from each part of the FRF matrix (Eq. 12) with

a roving sensor technique. After mass normalization, the modal shapes and the modal-shape slopes in Fig. 1 (Stage 3) are equal, regardless of whether they are obtained from force- or moment-excited response functions.

A complete dynamic analysis, including all of the existing modes, is available solely for analytical or numerical systems. Whenever the structure is analyzed experimentally, only a finite number of modes from a limited frequency range can be obtained. Dynamic responses below and above that range are not available, even though they exist in the structure. Inaccessible low- and high-frequency residuals are crucial in the FRF synthesis process. They mostly influence the anti-resonances, which are local characteristics between particular input and output measuring points. Even a small error in the synthesized FRF can lead to an erroneous result during the substructuring process. Extended notation of the general FRF synthesis equation, including the residuals effect, takes the following form:

$$\mathbf{h}_{ij}^{syn}(\omega) = -\frac{\mathbf{R}_{ij}^{LR}}{\omega^2} + \sum_{r=m_1}^{m_2} \frac{\phi_{ir} \phi_{jr}}{(\omega_r^2 - \omega^2) - j2\xi_r \omega_r \omega} + \mathbf{R}_{ij}^{UR}, \quad (13)$$

where lower and upper residuals are defined by:

$$-\frac{\mathbf{R}_{ij}^{LR}}{\omega^2} = \sum_{r=1}^{m_1-1} \frac{\phi_{ir} \phi_{jr}}{(\omega_r^2 - \omega^2) - j2\xi_r \omega_r \omega}, \quad (14)$$

$$\mathbf{R}_{ij}^{UR} = \sum_{r=m_2+1}^N \frac{\phi_{ir} \phi_{jr}}{(\omega_r^2 - \omega^2) - j2\xi_r \omega_r \omega}, \quad (15)$$

respectively, and  $\mathbf{h}_{ij}^{syn}(\omega)$  stands for the synthesized FRF matrix,  $\omega_r$  is the  $r$ -th natural frequency,  $\phi_{ir}$  and  $\phi_{jr}$  are the mass-normalized modal shape vectors and  $\xi_r$  is the  $r$ -th modal damping ratio. It is difficult to experimentally obtain the full DOF FRF matrix required in the FBS process. Therefore, the measured, force-excited part of the FRF matrix is transformed into a modal domain. The poly-reference MPE LSFD method enables us to estimate RBM and FM. The UR, widely discussed in [18], requires special consideration. They could be included from the equivalent numerical model or estimated from a measurement of all the necessary FRF curves in the range of interest. An alternative method was proposed by Ewins [19] to measure the FRFs high above the frequency range of interest. Due to the low modal density, in our simple structure, the inclusion of out-of-range modes sufficiently eliminates the UR effect.

#### 4. Quartz-based piezoelectric rotational accelerometer

There are several methods to measure the rotational response of a structure. Besides indirect methods, where rotations are estimated from measured translations, some direct methods are also available that are much more reliable and accurate. In this paper a quartz-based, piezoelectric, rotational accelerometer (Kistler type 8840) was used. Despite some alternative solutions based on micro-electromechanical systems (MEMS) [20], piezoresistive or bimorph [8] material, the dynamic performance of piezoelectric sensors is usually significantly better (Table 1).

Table 1: Technical data of quartz-based piezoelectric rotational accelerometer, Kistler type 8840.

Technical data	Units	Value
Acceleration Range	$\text{krad/s}^2$	$\pm 150$
Sensitivity	$\mu\text{V/rad/s}^2$	35.5
Frequency Response, $\pm 10\%$	Hz	1...2000
Resonant Frequency mounted	kHz	23
Transverse Sensitivity	%	1.5
Mass	grams	18.5

A rotational accelerometer (Fig. 2) is commonly used in car-safety tests and for the active control of oscillating shafts. A precise construction, the piezoelectric effect and a low cross sensitivity enable an effective measurement of rotations also in the field of structural dynamics. The interested reader is referred to [13] for additional information.

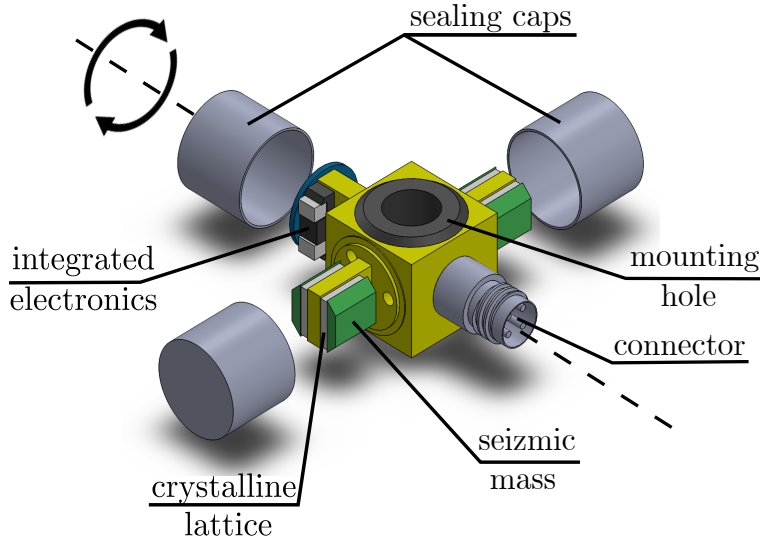


Figure 2: Inner construction of quartz-based piezoelectric rotational accelerometer.

## 5. Case study

The applicability of the proposed method is demonstrated on a simple beam structure. The rectangular cross-section beam AB represents the main system, which is divided into the two unequally long subsystems A and B during the substructuring process (Fig. 3). In this paper the dynamic response of the beam AB will be obtained by coupling the dynamics of its two subsystems. Even though a very simple system is analyzed, several difficulties occur due to the measured FRFs associated with the rotational degrees of freedom. The geometry and material properties of the system and both subsystems are presented in Table 2. The beam A was discretized with 7 and beam B with 5 uniformly distributed nodes. For each node the translational acceleration in the  $y$  direction and the rotational acceleration around the  $z$  axis were measured. The free-free boundary conditions were considered. The presented case study is completely based on the experimentally obtained data. At each step of the process, the quality of the experimental data are compared with the reference numerical model.

Although the structure in case study presents a frequently analyzed system within EMA, several issues had to be resolved in order to obtain reliable measurements. Generally, two sources of errors can be introduced during the measurements. First, there are the random errors that introduce uncertainty

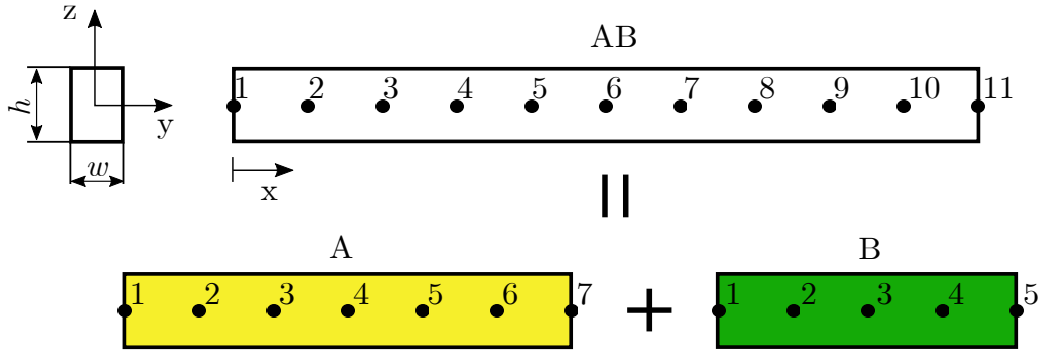


Figure 3: Division of beam AB into the subsystems A and B with node numbers and definition of the cross-section.

Table 2: System's geometrical and material properties.

Parameter	Units	Value
A	mm	600
B	mm	400
AB	mm	1000
$w$	mm	30
$h$	mm	50
$\rho$	kg/m <sup>3</sup>	7933
E	GPa	210

into the measured data that are normally not under control. The second type are the bias or systematic errors. Here, the errors introduce systematically shifted values of the resonances and anti-resonances. The interested reader can find more about errors in [21, 22].

In order to reduce the bias errors, extra attention was focused on the selection of the appropriate length and type of ropes that represent the free-free boundary conditions. This strongly impacts on the rigid-body modes and, consequently, on the positions of the anti-resonances. The force excitation was performed with a rail-guided modal hammer (Fig. 4) to provide an accurate force impact location. The translational and rotational accelerations were measured with precisely positioned, oriented and calibrated piezoelectric accelerometers to minimize the cross sensitivity. The mass of the attached sensors was compensated with dummy masses at all the measurement locations and sequentially replaced with a roving accelerometer.

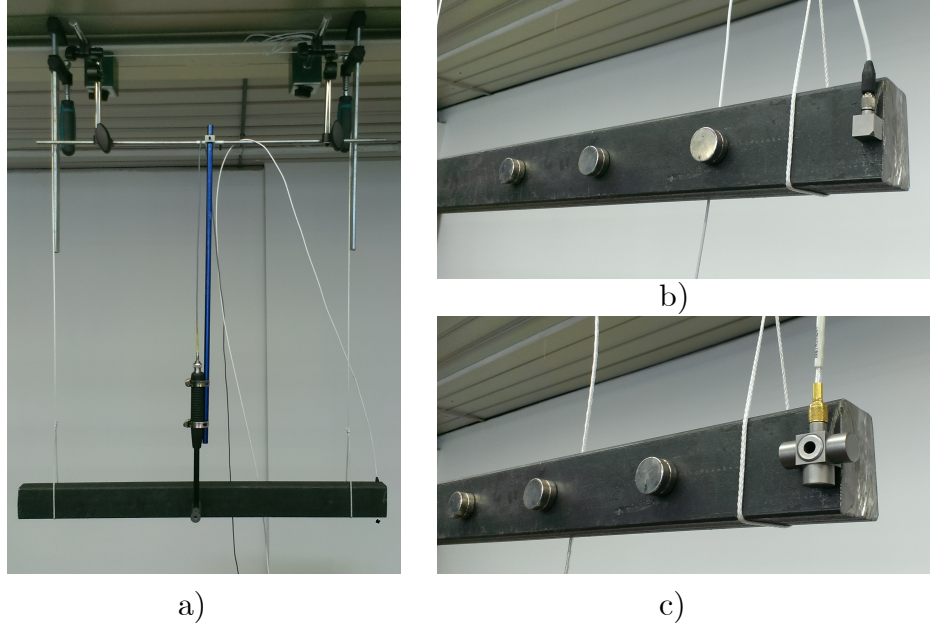


Figure 4: Experimental setup of subsystem A; a) Rail-guided impact hammer and free-free boundary conditions, b) Translational accelerometer, c) Rotational accelerometer.

During the signal processing an additional error can be introduced. Modal truncation is certainly one of the major issues when dealing with EMA. It is impossible to obtain all modal shapes and include them into the substructuring process. Beside flexible modes, also rigid-body modes and upper residuals need to be considered.

Applying the proposed procedure to both subsystems results into two full DOF FRF matrices  $\mathbf{Y}_A$  and  $\mathbf{Y}_B$ . They are then combined together into a single matrix, defined as:

$$\mathbf{Y}(\omega) = \begin{bmatrix} \mathbf{Y}_A & \mathbf{0} \\ \mathbf{0} & \mathbf{Y}_B \end{bmatrix}, \quad (16)$$

which is inserted into Eq. (9). The connection between both subsystems is rigid, which can be expressed with Boolean mapping matrix as:

$$\mathbf{B} = \begin{bmatrix} 1_y^A & 1_{rz}^A & 2_y^A & 2_{rz}^A & \dots & 7_y^A & 7_{rz}^A & 1_y^B & 1_{rz}^B & \dots & 5_y^B & 5_{rz}^B \\ 0 & 0 & 0 & 0 & \dots & 1 & 0 & -1 & 0 & \dots & 0 & 0 \\ 0 & 0 & 0 & 0 & \dots & 0 & 1 & 0 & -1 & \dots & 0 & 0 \end{bmatrix}, \quad (17)$$

where one boundary node for each subsystem is coupled with two degrees of freedom.

The analyzed frequency range is conditioned by the technical specifications of the measurement equipment. The frequency range is defined by a rotational accelerometer, which is calibrated between 1 and 2000 Hz. However, preliminary measurements revealed very good agreement between the FRFs and the numerical model up to 4100 Hz, which was set as the upper limit in all the measurements. Within the frequency range, a relatively small modal density, (4 FM in the subsystem A and 3 FM in the subsystem B) appears. The fifth FM for subsystem A and the fourth FM for B appear at 5872 Hz and 5350 Hz, respectively. Those two have some influences on the lower frequency range, but almost negligible influence below 1600 Hz. The latter frequency was set as the upper limit in the following results. The ability to measure the dynamical response of a simple beam structure high above the interval of interest makes it possible to successfully perform the required FRF synthesis.

### *5.1. Substructuring results*

The proposed dynamic substructuring process is divided into four steps: measurement, curve fitting, FRFs synthesis and final coupling. The main difficulty with the experimental dynamic substructuring methods is the quality of the measured FRFs. It is well known that the substructuring process is effective and reliable whenever the FRFs are obtained based on numerical or analytical models [2, 23]. Therefore, good agreement between the measured and the numerically obtained FRFs is essential to successfully perform an experimentally based substructuring process. Thus, numerically obtained FRFs based on a finite-element model (FEM) are presented in order to estimate the quality of the measured FRFs and to finally show the influence of real measurement data on the quality of the substructuring algorithm. To simplify the presentation, all the intermediate results and observations are related only to the subsystem A.

Figure 5 shows the subsystem A driving- and transfer-point FRFs for the translational and rotational acceleration response. The positions, shapes and amplitudes of the resonance as well as the anti-resonance regions are in good agreement with the numerical model. The random noise in rotational FRFs is present mostly due to the rotational accelerometer's characteristics. Even though a special effort was made with the experimental setup, a small amplitude peak can be observed around 730 Hz in Figure 5 d. It is related

to the dynamic response of the beam in the  $z$  direction that appears as the cross-sensitivity effect also in the  $y$  direction. As will be shown later, it does not significantly affect the quality of the final results.

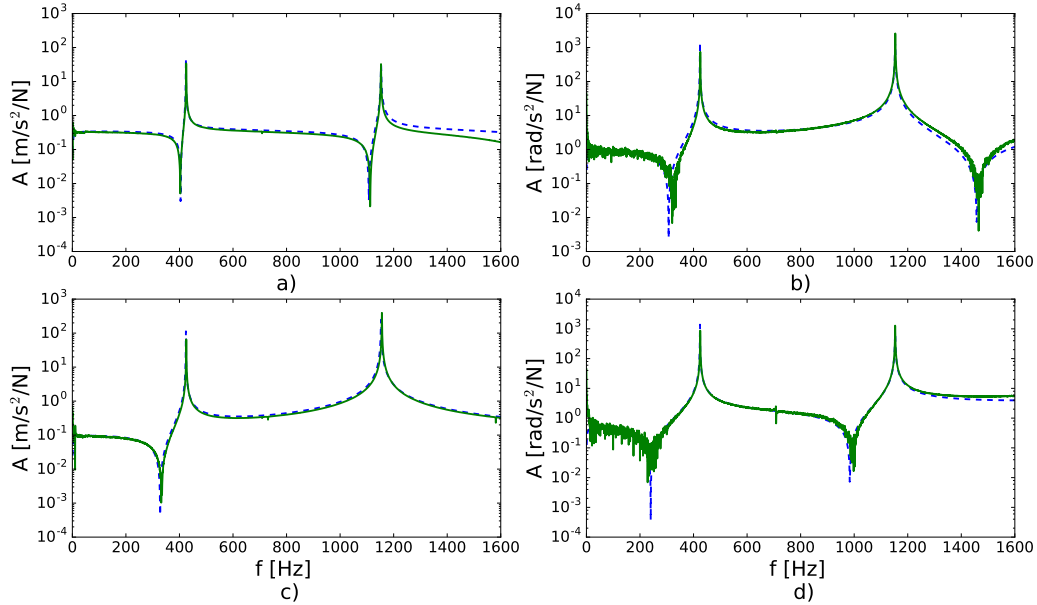


Figure 5: Comparison between numerically (—•—) and experimentally (—) obtained FRFs; a)  $\text{FRF}_{2y2y}$ , b)  $\text{FRF}_{2y2rz}$ , c)  $\text{FRF}_{3y5y}$ , d)  $\text{FRF}_{3y5rz}$ .

The modal parameters were estimated based on five columns in the FRF matrix (force excitation from nodes 2 to 6 on the beam A) with the poly-reference LSFD MPE method. First, three mass-normalized modal shapes and modal-shape slopes are presented in Fig. 6. Good agreement between the experimentally and numerically obtained modal shapes was observed due to the high quality of the measured FRFs. Rigid-body modes were also estimated from the measurements, while the contribution of the upper residuals was indirectly included by accounting for higher flexible modal shapes in the FRF synthesis process.

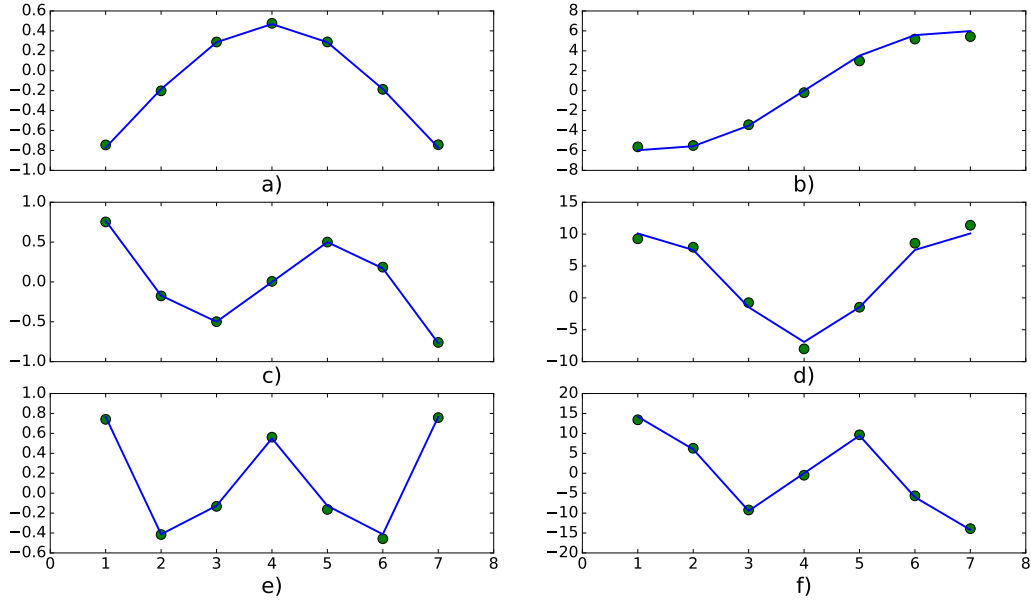


Figure 6: Comparison of numerical (—) and experimental (•••) modal shapes (MS) and modal-shape slopes (MSS); a) MS-1, b) MSS-1, c) MS-2, d) MSS-2, e) MS-3, f) MSS-3.

The experimentally obtained RBM and FM were used in Eq. (13) to synthesize the FRFs in all four quadrants of the FRF matrix. A couple of results from each quadrant are shown in Fig. 7 and Fig. 8. With the FRF synthesis a random noise is eliminated and a satisfactory correlation with the numerical data is obtained. Anti-resonances are slightly shifted, mainly due to the errors in the estimated RBM and the compensation of UR with modes outside the range of interest. Comparing the force-excited experimental FRFs in Fig. 5 with the synthesized FRFs in Fig. 7 it seems that the regenerated FRFs are less accurate than those measured directly. The actual difference is in the range of  $0.05 \text{ m/s}^2/\text{N}$ , which escalates due to the logarithmic scale on the amplitude axis. Nevertheless, the quality of the synthesized force- and moment-excited FRFs is acceptable.

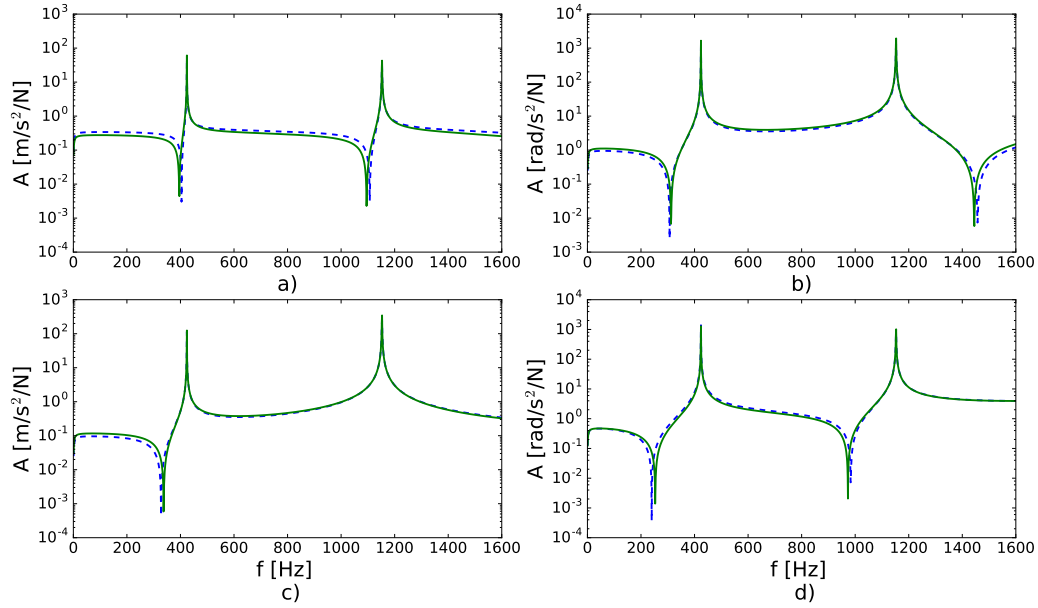


Figure 7: Comparison of numerical (---) and synthesized (—) FRFs; a)  $FRF_{2y2y}$ , b)  $FRF_{2y2rz}$ , c)  $FRF_{3y5y}$ , d)  $FRF_{3y5rz}$ .

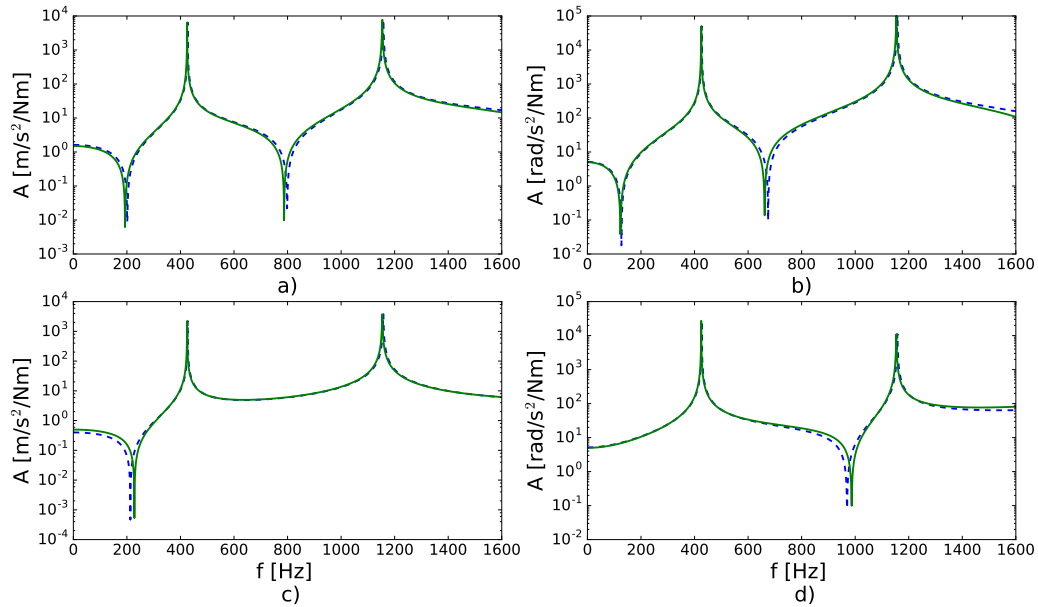


Figure 8: Comparison of numerical (---) and synthesized (—) FRFs; a)  $FRF_{1rz1y}$ , b)  $FRF_{1rz1rz}$ , c)  $FRF_{2rz5y}$ , d)  $FRF_{2rz5rz}$ .

The final results of the coupled subsystems A and B in Fig. 9 are compared with references based on the numerical model and the measured FRFs of the system AB. The resonance and anti-resonance frequencies are slightly shifted, moreover the amplitudes are not in complete agreement with the references. Although the coupled FRFs do not match perfectly with the references, the proposed procedure with the included measured rotations provide relatively good results in a particular case study. The quality of the results can be additionally improved by upgrading the procedure with numerically supported algorithms like the VIKING method [11].

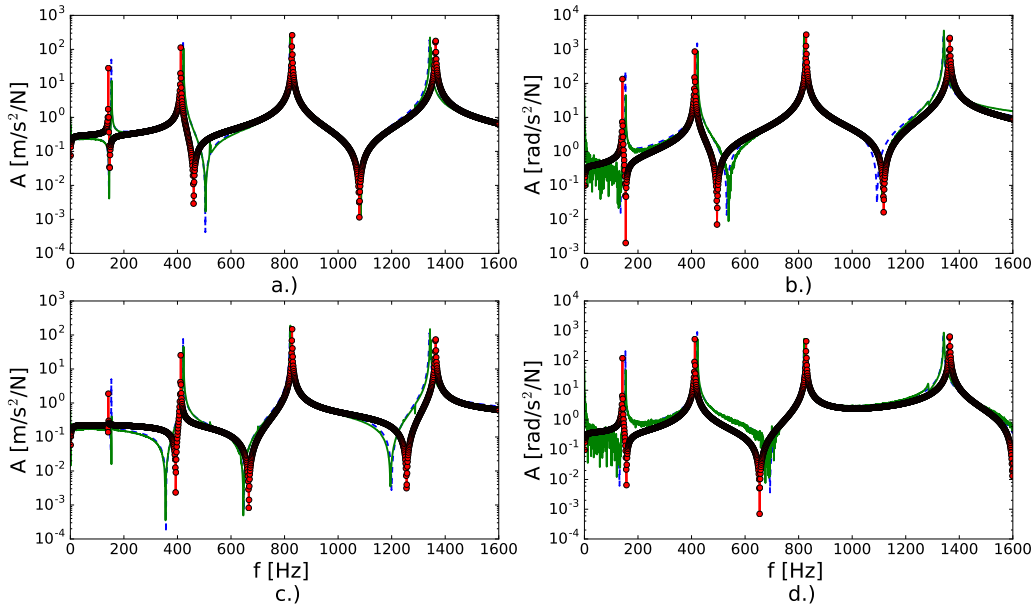


Figure 9: Comparison between coupled ( $\bullet$ ), numerically ( $-\cdot-$ ) and experimentally ( $—$ ) obtained FRFs of system AB; a)  $\text{FRF}_{3y1y}$ , b)  $\text{FRF}_{3y1rz}$ , c)  $\text{FRF}_{3y3y}$ , d)  $\text{FRF}_{3y3rz}$ .

## 6. Conclusions

This paper presents a method to obtain a full-degrees-of-freedom FRF matrix based on measurements to effectively perform a frequency-based substructuring process. For measuring the rotations a quartz-based, piezoelectric, rotational accelerometer was used. The response model was expanded with a modal model and implemented in the LM FBS method. The applicability of the proposed method was demonstrated in a case study where

the dynamic response of a steel-beam system was obtained by coupling the dynamic responses of its two subsystems. Even though the coupled FRFs do not match perfectly with the references, very promising results can be achieved by the inclusion of measured rotations in the proposed method. For more complex applications, an additional improvement can be implemented by upgrading the proposed method with numerical updating algorithms.

## References

- [1] D. de Klerk, D. J. Rixen, J. de Jong, The Frequency Based Substructuring (FBS) Method reformulated according to the Dual Domain Decomposition Method, in: Proceedings of the XXIV International Modal Analysis Conference, St. Louis, MO, Society for Experimental Mechanics, Bethel, CT, 2006.
- [2] B. Jetmundsen, R. L. Bielawa, W. G. Flannelly, Generalized Frequency Domain Substructure Synthesis, *Journal of the American Helicopter Society* 33 (1) (1988) 55–64.
- [3] S. S. Sattinger, Method for Experimentally Determining Rotational Mobilities of Structures, *The Journal of the Acoustical Society of America* 50 (6) (1980) .
- [4] S. Jianxin, C. Mak, Direct measurement of moment mobility and a moment excitation system, *Applied Acoustics* 63 (2) (2002) 139–151.
- [5] P. Varoto, M. Lofrano, T. Cicogna, L. Oliveira, Moment Mobility FRF Measurement Techniques, in: Proceedings of the XXIV International Modal Analysis Conference, St. Louis, MO, Society for Experimental Mechanics, Bethel, CT, 2006.
- [6] A. S. Elliott, A. T. Moorhouse, G. Pavić, Moment excitation and the measurement of moment mobilities, *Journal of Sound and Vibration* 331 (11) (2012) 2499–2519.
- [7] Y. Champoux, V. Cotoni, B. Paillard, O. Beslin, Moment excitation of structures using two synchronized impact hammers, *Journal of Sound and Vibration* 263 (3) (2003) 515–533.

- [8] M. Bello, A. Sestieri, W. D'Ambrogio, F. La Gala, Development of a rotation transducer based on bimorph PZTS, *Mechanical Systems and Signal Processing* 17 (5) (2003) 1069–1081.
- [9] Y. Y. Kim, J. H. Kang, A New Experimental Method to Determine Rotational Modes from the Strain Measurement, in: *Proceedings of SPIE - The International Society for Optical Engineering*, Orlando, FL, Society for Experimental Mechanics, Bethel, CT, 1997, pp. 1415–1418.
- [10] A. Sestieri, W. D'Ambrogio, R. Brincker, A. Skafte, A. Culla, Estimation of Rotational Degrees of Freedom by EMA and FEM Mode Shapes, in: *Special Topics in Structural Dynamics, Volume 6, Conference Proceedings of the Society for Experimental Mechanics Series*, Springer New York, 2013, pp. 355–365.
- [11] L. Thibault, A. Butland, P. Avitabile, Variability Improvement of Key Inaccurate Node Groups – VIKING, in: *Topics in Modal Analysis II, Volume 6, Conference Proceedings of the Society for Experimental Mechanics Series*, Springer New York, 2012, pp. 603–624.
- [12] D. de Klerk, D. J. Rixen, S. N. Voormeeren, F. Pasteuning, Solving the RDoF Problem in Experimental Dynamic Substructuring, in: *Proceedings of the XXVI International Modal Analysis Conference*, Orlando, FL, Society for Experimental Mechanics, Bethel, CT, 2008.
- [13] M. Dumont, N. Kinsley, Rotational Accelerometers and Their Usage in Investigating Shaker Head Rotations, in: *Proceedings of the Society for Experimental Mechanics Series*, Springer International Publishing, 2015, pp. 85–92.
- [14] M. N. M. Maia, *Theoretical and Experimental Modal Analysis*, Research Studies Pre, Taunton, Somerset, England : New York, 1997.
- [15] D. J. Ewins, *Modal Testing, Theory, Practice, and Application*, 2nd Edition, Research Studies Press, Baldock, Hertfordshire, England ; Philadelphia, PA, 2000.
- [16] T. R. Sutter, C. J. Camarda, J. L. Walsh, H. M. Adelman, Comparison of several methods for calculating vibration mode shape derivatives, *AIAA Journal* 26 (12) (1988) 1506–1511.

- [17] S. Adhikari, Calculation of derivative of complex modes using classical normal modes, *Computers & Structures* 77 (6) (2000) 625–633.
- [18] M. L. M. Duarte, Experimentally-derived structural models for use in further dynamic analysis, Ph.D. thesis, University of London, Imperial College of Science, Technology and Medicine, London (1996).
- [19] D. J. Ewins, Modal Test Requirements for Coupled Structure Analysis Using Experimentally-Derived Component Models, in: *ASCE/ASME Mechanics Conference*, American Society of Mechanical Engineers, New York, 1985.
- [20] A. Gola, E. Chiesa, E. Lasalandra, F. Pasolini, M. Tronconi, T. Ungaretti, A. Baschiroto, Interface for MEMS-based rotational accelerometer for HDD applications with 2.5 rad/s<sup>2</sup> resolution and digital output, *IEEE Sensors Journal* 3 (4) (2003) 383–392.
- [21] D. de Klerk, How Bias Errors Affect Experimental Dynamic Substructuring, in: *Proceedings of the 28th International Modal Analysis Conference (IMAC XXVIII)* Jacksonville, FL, Springer New York, 2011, pp. 1101–1112.
- [22] D. de Klerk, S. N. Voormeeren, Uncertainty Propagation in Experimental Dynamic Substructuring, in: *Proceedings of the Twenty Sixth International Modal Analysis Conference*, Orlando, FL, Society for Experimental Mechanics, Bethel, CT, 2008.
- [23] Y. Ren, C. F. Beards, On substructure synthesis with FRF data, *Journal of Sound and Vibration* 185 (5) (1995) 845–866.